

Mesoscopic dynamics of piezoelectric copolymer thin films

Mahapatra, D.R. and Melnik, R.V.N.

**Smart Structures and Materials 2006: Electroactive Polymer
Actuators and Devices (EAPAD), Ed. Y. Bar-Cohen,
Proceedings of SPIE, Vol. 6168, San Diego, Feb 26- March 2,
61682D-1--61682D-10 (10 pages), 2006.**

Mesoscopic Dynamics of Piezoelectric Copolymer Thin Films

D. Roy Mahapatra and R.V.N. Melnik

Mathematical Modelling and Computational Sciences,
Wilfrid Laurier University, Waterloo, ON, N2L3C5, Canada

ABSTRACT

A mesoscopic model to analyze various effects of electroactive and flow related properties in piezoelectric copolymer composite thin film has been developed in this paper. A three-phase composite with piezoelectric particulate phase, electroactive polymer phase and graft polymer-matrix phase is considered. The homogenized constitutive model takes into account the local transport of cations in polymer, electrostriction and anhysteretic polarization. A finite strain description is given which includes the mesoscopic dispersion of copolymer chains. Finite element simulation is carried out by considering a P(VDF-TrFE)-PZT-Araldite thin film. Analysis of the results indicate that an increasing copolymer content substantially changes the deformation pattern in the film.

Keywords: Piezoelectric, polymer, mesoscopic, finite strain, thin film.

1. INTRODUCTION

Polymer semiconductors and their composite variants with significant piezoelectric effect are considered as promising candidates to compete with the silicon based technology. Piezoelectric copolymer composite films, such as ultra-thin Langmuir-Boldgett films of PVDF and its copolymer with trifluoroethylene (P(VDF-TrFE)),¹ ionic polymer² and electrostrictive elastomers³ have several potential applications, especially in photonics, biomedical devices, macromolecular assembly and smart structures. The category of polymer composite we are interested in this paper is the one in which the piezoelectricity, the electrical charge and the polymer dispersion interplay to produce a desired functionality. Detailed discussions on the merits and demerits of various piezoelectric copolymer composites can be found in published literature (see references^{2,4,5}). Computational models have been developed in literature for polymer chains in solvent as they are solidified (see reference⁶). Substantial efforts have been devoted to the analysis of the equilibrium conformations of the polymer chains and their interactions in a non-Newtonian fluid. In the solid state, the dynamics of the piezoelectric copolymer (thin film) is governed by the deformation of the polymer chains which also undergo electrical polarization and transport of charge. Due to this coupled dynamics, the charge transport with dynamical changes in the conduction band of the polymeric network is of importance in photonics related applications. On the other hand, electrostriction induced mechanical motion and flexibility of the piezoelectric copolymer film is of importance for smart structural applications. Molecular level modeling of the dynamics and related observations have been reported in literature.^{7,8} Macroscopic effect of linear piezoelectricity and electrostriction in piezoelectric composite structures have been studied widely. However, in polymer composite, various effects which are important for small scale applications (e.g. flexible thin film device) have not been well reported in literature. In this paper, we develop a mesoscopic model to study these effects.

The outline of the paper is the following. In Sec. 2 we derive a constitutive model of a three-phase composite with piezoelectric particulate, electroactive polymer and elastomeric matrix. In Sec. 3 we give a kinematic description of the composite including the dispersion of the copolymers. The dynamics aspect is discussed in Sec. 4. In Sec. 5 we perform numerical simulation of mechanical deformation by considering P(VDF-TrFE)-PZT-Araldite thin film.

Further author information: (Send correspondence to D.R.M.)
D.R.M.: E-mail: droymahapatra@wlu.ca, Telephone: 1 519 884 0710 ext. 3019
R.V.N.M.: E-mail: rmelnik@wlu.ca, Telephone: 1 519 884 0710 ext. 3662

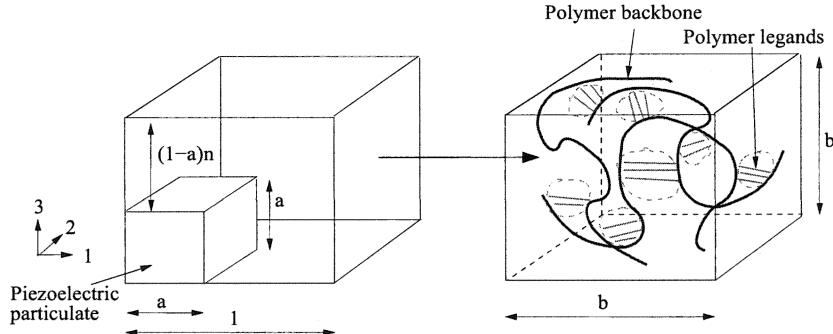


Figure 1. Schematic representation of the piezoelectric copolymer composition.

2. CONSTITUTIVE MODEL

Here, we first discuss a general formulation of the piezoelectric polymer composite thin film problem. Electrical excitation to the film is generally given by surface electrodes. From the microscopic viewpoint, the mechanism of electrical excitation by electrode is not well defined. This is due to the fact that electrode material remains in a diffused state with the polymeric system and there is a lack of crystalline surfaces. Therefore, at the microscopic scale, the interaction is three-dimensional. On the other hand, for device level analysis and design optimization, a thin film type geometry requires a reduced dimensional model. By a mesoscopic modeling approach, we reduce the problem complexity from a three-dimensional polymeric composite system by reducing the details of the polymer dispersion and by applying appropriate boundary condition for deformation and electromagnetic fields in the thin film limit. In order to derive the dynamics in this mesoscopic modeling approach, we first construct a three-dimensional constitutive model and homogenize corresponding to a quasi-three dimensional situation.

We define the Cartesian components of stress (σ), strain (ϵ), electric charge displacement (D), electric field intensity (E), magnetic flux (B) and the magnetic field intensity (H) in (x, y, z) . Our objective is to construct a constitutive model of the form

$$\sigma = c\epsilon + \tau c'\dot{\epsilon} - \tau\dot{\sigma} - \sigma(E)_p, \quad (1a)$$

$$D = \epsilon E + P(\epsilon, E), \quad (1b)$$

$$B = \mu H + \mu_0 M(\epsilon), \quad (1c)$$

where c is the stiffness, c' is the flow coefficient, τ is a strain relaxation time constant, σ_p is the electric polarization induced stress, ϵ is the dielectric permittivity, P is the electrical polarization vector due to transformation and deformation of the macro-molecular structure, μ is the magnetic permeability and M is the magnetic polarization vector due to molecular spin. There can be several other effects depending on the composition of the piezoelectric polymer (e.g., inclusion of ferromagnetic particles, inclusions of left-handed material systems with negative index etc.), however increasing complexities in this way would restrict the use of experimentally measured material constants, since such experiments are performed on bulk sample without the effects of constraints on domain formation. The only straightforward yet computationally prohibitive method is then to perform molecular dynamic simulations. With the basic assumptions on the nature of the coupling among the mechanical and the electromagnetic field in Eqs. (1a)-(1c), we next consider individual structure of the linear and the nonlinear parts in the constitutive model.

We split the total charge density ρ_{total} and the total conduction current J_{total} as

$$\rho_{\text{total}} = \rho_c + \rho_p \quad J_{\text{total}} = J + J_p + J_m, \quad (2)$$

where ρ_c is the true charge density, ρ_p is the bound charge density, J is the true conduction current, J_p is the conduction current due to bound charge, J_m is the molecular current density. The local conservation laws are then

$$\nabla \cdot P = -\rho_p, \quad \nabla \times M = J_m, \quad (3)$$

and the local continuity condition reads

$$\nabla \cdot \mathbf{J}_p = -\dot{\rho}_p . \quad (4)$$

ρ_c is related to the conduction current \mathbf{J} by the continuity condition

$$\nabla \cdot \mathbf{J} = -\dot{\rho}_c . \quad (5)$$

Eq. (5) has important to consider mainly for polymer semiconductor and chemically active electroactive polymers and gels. The bound charge density ρ_p is obtained from the molar concentration (c_n) of cations and the molar concentration (c_{group}) of charge groups in the polymer (e.g. sulfonic or carboxylic groups in ionic polymer composite²), which can be written as

$$\rho_p = (c_n - c_{\text{group}})Ne , \quad (6)$$

where N is the Avogadro's number and e is the elementary charge of an electron. Further, the migration of cations can be important for certain polymers, which should then follow the Onsagar theory or irreversible thermodynamics. Neglecting the piezoelectric coupling in the constitutive model in Eqs. (1a)-(1c) for this local thermodynamics, one can write the ion transport equation as

$$\mathbf{J}_p = \sigma_c \mathbf{E} - \mathbf{L} \nabla p , \quad (7)$$

and the solvent transport equation as

$$\mathbf{Q} = \mathbf{L}^T \mathbf{E} - K \nabla p , \quad (8)$$

where $p = \frac{1}{3} \text{Tr}(\boldsymbol{\sigma})$ is the hydrostatic stress, \mathbf{Q} is the solvent flux, σ_c is the electric conductance, K is the Darcy permeability and \mathbf{L} is a symmetric positive definite coefficient matrix obtained experimentally. Assuming that the solvent flux is negligible for solid-state applications, the local conservation equation due to migrating charge is expressed as

$$e \mathbf{E} \approx kT \nabla (\ln(c_n)) , \quad (9)$$

where k is the Boltzman constant, T is the temperature. With the help of Eqs. (7) and (9) in Eq. (6), the continuity equation for the migrating charge finally becomes

$$\overline{(c_n N)} e = \frac{\sigma_c}{e} kT \nabla^2 [\ln(c_n)] - \frac{1}{3} \nabla \cdot (\mathbf{L} \nabla [\text{Tr}(\boldsymbol{\sigma})]) . \quad (10)$$

Further, for piezoelectric polymer blends, it is reasonable to adopt an averaging approach to obtain the true charge density and the effective dielectric properties. To this end, for the present study, we also neglect spin polarized current, i.e. $J_m = 0$. Since in polymer blends, the poling can be done through network of metallic wires embedded in the solidified matrix phase, the conduction current induced charge density can have special distribution depending on the type of interaction between the piezoelectric particles, the polymer-metal legands. The true charge density is assumed to be

$$\rho_c = \nu_{\text{co}}(\rho_c)_{\text{co}} + \nu_{\text{pa}}(\rho_c)_{\text{pa}} , \quad (11)$$

where ν_{co} and ν_{pa} are respectively the volume fraction corresponding to the copolymers and piezoelectric particles and they satisfy the relation

$$\nu_{\text{co}} + \nu_{\text{el}} = \frac{a + (1-a)n - a^2}{a + (1-a)n} , \quad \nu_{\text{pa}} = \frac{a^2}{a + (1-a)n} . \quad (12)$$

With reference to Fig. 1, ν_{el} is the volume fraction of the elastomeric matrix. For piezoelectric composite thin film, it is convenient to consider the 0-3 connectivity. We employ the method of effective property calculation as reported by Banno and Saito,⁹ which is found to be effective for 0-3 composite with ellipsoidal inclusions. We write the effective dielectric constant as

$$\epsilon = \mathbf{I}\epsilon , \quad \epsilon = \frac{a^2[a + (1-a)n]^2\epsilon_1\epsilon_{\text{pa}}}{a\epsilon_{\text{pa}} + (1-a)n\epsilon_1} + \{1 - a^2[1 + (1-a)n]\}\epsilon_{\text{pa}} , \quad (13)$$

where ϵ_1 is the effective dielectric constant for the copolymer-matrix, which is assumed to be

$$\epsilon_1 = \nu_{\text{co}}\epsilon_{\text{co}} + \nu_{\text{el}}\epsilon_{\text{el}} . \quad (14)$$

ϵ_{pa} , ϵ_{co} and ϵ_{el} are the dielectric constants for the piezoelectric particulate, copolymer and matrix, respectively. The magnetic permeability is expressed as

$$\boldsymbol{\mu} = \mathbf{I}\boldsymbol{\mu}, \quad \boldsymbol{\mu} = \nu_{\text{pa}}\mu_{\text{pa}} + \nu_{\text{co}}\mu_{\text{co}} + \nu_{\text{el}}\mu_{\text{el}}, \quad (15)$$

where μ_{pa} , μ_{co} and μ_{el} are magnetic permeability for the piezoelectric particulate, copolymer and matrix, respectively.

We now consider the calculation of effective stiffness, piezoelectric coupling and electrostriction. It should be noted that crystallinity may not exist for the polymer composite such as the three-phase system considered here. The constitutive behaviour can be anisotropic. However, for thin film type geometry, it is not practical to include the full anisotropy. Here we consider stiffness with monoclinic type for piezoelectric particulate, which is written as

$$\mathbf{c}_{\text{pa}} = \begin{bmatrix} c_{11} & c_{12} & c_{13} & 0 & 0 & c_{16} \\ c_{12} & c_{22} & c_{23} & 0 & 0 & c_{26} \\ c_{13} & c_{23} & c_{33} & 0 & 0 & c_{36} \\ 0 & 0 & 0 & c_{44} & c_{45} & 0 \\ 0 & 0 & 0 & c_{54} & c_{55} & 0 \\ c_{16} & c_{26} & c_{36} & 0 & 0 & c_{66} \end{bmatrix}. \quad (16)$$

The reference frame axes of the volume element are parallel to the global coordinate, where 3 indicates the direction normal to the film plane. The matrix phase is assumed to be isotropic with stiffness matrix denoted by \mathbf{c}_{el} in the coordinate system of the volume element. The polymer phase is modeled by one-dimensional chains with their orientation angle $\theta(x, y)$ of the backbone as shown in Fig. 2. The chain is extensible with small shear stiffness. The stiffness matrix for the chain in the coordinate system corresponding to the volume element is expressed as

$$\mathbf{c}_{\text{co}} = \boldsymbol{\Gamma}(\theta)^T \mathbf{c}_{\text{chain}} \boldsymbol{\Gamma}(\theta), \quad (17)$$

where $\boldsymbol{\Gamma}(\theta)$ is the transformation matrix for the symmetric fourth rank tensor. With the introduction of individual forms of the electrostriction and polarization, which is discussed next, we perform averaging of the stiffness and the piezoelectric properties considering linear parts of the constitutive model. This is done by taking into account the 0-1, 0-2 average correction on the effective dielectric constant derived in Eq. (13). For analysis of the thin film, we use a plane-stress type approximation with the assumption of parallel electrode on the film surfaces.

The polarization induced stress in the constitutive model in Eq. (1a) is considered to be of the following form

$$\boldsymbol{\sigma}(\mathbf{E})_p = \mathbf{e}^T \mathbf{E} + cQ\epsilon_0^2(\boldsymbol{\epsilon} - \mathbf{I})^2 \begin{bmatrix} 1 & 0 & 0 \\ 0 & 1 & 0 \\ 0 & 0 & 0 \end{bmatrix} E_z^2 + \epsilon_0^2 \boldsymbol{\epsilon} \begin{bmatrix} 1 & 0 & 0 \\ 0 & 1 & 0 \\ 0 & 0 & 0 \end{bmatrix} E_z^2, \quad (18)$$

where \mathbf{e} is the effective piezoelectric coefficient matrix obtained by averaging of the three-phase linear model, Q is the electrostrictive coefficients. In Eq. (18), the second term describes the stress due to electrostriction and the third term describes the Maxwell stress. The polarization vector \mathbf{P} is considered to be of the following form

$$\mathbf{P}(\boldsymbol{\epsilon}, \mathbf{E}) = \mathbf{e}\boldsymbol{\epsilon} + \boldsymbol{\Gamma}(\theta)^T P_s \tanh\left(\frac{E_e}{a}\right) \boldsymbol{\Gamma}(\theta)', \quad (19)$$

where the first term describes the electric displacement due to polarization of the predominantly piezoelectric particulate-matrix phase and the second term describes the anhysteretic polarization of the oriented polymer chain constrained by the piezoelectric particulate-matrix phase, which is based on Ising-spin relation.¹⁰ Here $\boldsymbol{\gamma}(\theta)'$ is the vector transformation matrix, P_s is the saturation polarization, E_e is the effective electric field acting along the dipole moment and is expressed as

$$E_e = E_{||} + \alpha P_s \tanh\left(\frac{E_e}{a}\right), \quad (20)$$

$\alpha = \hat{E}/P_s$ with \hat{E} as the scaling electric field, and a is a constant given by $a = \hat{E}T/(3T_c)$ where T_c is the Curie temperature of the composition. \hat{E} , a and α are to be estimated from experimental data. The parallel electric field $E_{||}$ is related to the components of the electric field vector in the film coordinate (see Fig. 2) as

$$E_{||} = \sqrt{E_x^2 + E_y^2} . \quad (21)$$

3. MESOSCOPIC KINEMATICS

Having defined various terms in the constitutive model, the main task is now to derive the kinematics of the three-phase composite at the mesoscopic scale. Here we first define the displacement field as

$$\mathbf{u} = \mathbf{u}_{\text{ep}} + \frac{1}{m} \sum_{i=1}^m \mathbf{v}_i , \quad (22)$$

where $\mathbf{u}_{\text{ep}} = \{u_x \ u_y \ u_z\}^T$ denotes the displacement vector due elastic deformation of the predominantly piezoelectric particulate-matrix phase, m is the number of copolymer chains present in the volume element, \mathbf{v}_i denotes displacement due to the kinematics of the segment of the chain with length $m'a_0$ centered at a material point i with coordinate (x_i, y_i) , where m' is the number of blocks in the segment of the chain and a_0 is the C-C bond length in the backbone. The segment of the chain is assumed to be oriented at an angle $\theta_i = \theta$ as shown in Fig. 2(b). The kinematics of the segment can be described as

$$\mathbf{v}_i = m'a_0 [1 - \cos(\theta(x_i, y_i)_i - \theta(x_i, y_i)_i^0)] \begin{Bmatrix} \cos \theta(x_i, y_i)_i^0 \\ \sin \theta(x_i, y_i)_i^0 \\ 0 \end{Bmatrix} , \quad (23)$$

where $\theta(x_i, y_i)_i^0$ denotes the saturation conformation under the applied mechanical and electrical loading. In general, the flow in the copolymer phase in terms of its distribution \mathbf{v}_i should follow a kinetic law (e.g. Smoluchowski equation of disperse colloidal system.⁶) However, solving the mesoscopic dynamics including this dispersion effect is not an easy task. Instead, in the present model we prescribe the distribution of the saturation conformation in terms of θ_i^0 and solve the equations of motion.

The finite strain $\boldsymbol{\epsilon}$ is expressed as

$$\boldsymbol{\epsilon} = \frac{1}{2} [\nabla \mathbf{u} + (\nabla \mathbf{u})^T + (\nabla \mathbf{u})^T \nabla \mathbf{u}] . \quad (24)$$

With the help of Eq. (25) in Eq. (24) and neglecting the small order term, we arrive at the following form

$$\begin{aligned} \boldsymbol{\epsilon} \approx \frac{1}{2} & \left[\nabla \mathbf{u}_{\text{ep}} + (\nabla \mathbf{v})_{\text{ep}}^T + \frac{1}{m} \sum_{i=1}^m \nabla \mathbf{v}_i + \frac{1}{m} \sum_{i=1}^m (\nabla \mathbf{v}_i)^T + \frac{1}{m} \left(\sum_{i=1}^m \nabla \mathbf{v}_i \right)^T \nabla \mathbf{u}_{\text{ep}} + \frac{1}{m} (\nabla \mathbf{u}_{\text{ep}})^T \left(\sum_{i=1}^m \nabla \mathbf{v}_i \right) \right. \\ & \left. + \frac{1}{m^2} \left(\sum_{i=1}^m \nabla \mathbf{v}_i \right)^T \left(\sum_{i=1}^m \nabla \mathbf{v}_i \right) \right] . \end{aligned} \quad (25)$$

4. EQUATIONS OF MOTION.

The momentum conservation equation is expressed as by keeping the electrostriction induced terms on the right hand side as coupling term.

$$\rho \frac{\partial^2 \mathbf{u}}{\partial t^2} - \nabla \cdot \boldsymbol{\sigma} = \mathbf{0} , \quad (26)$$

where the effective mass density $\bar{\rho}$ is given by

$$\bar{\rho} = \nu_{\text{el}}(\bar{\rho})_{\text{el}} + \nu_{\text{pa}}(\bar{\rho})_{\text{pa}} + \nu_{\text{co}}(\bar{\rho})_{\text{co}} . \quad (27)$$

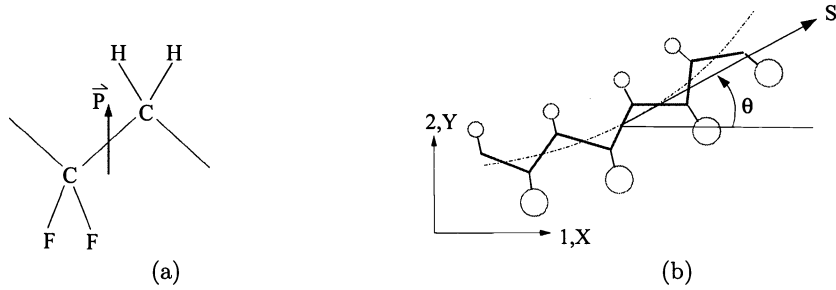


Figure 2. (a) PVDF molecular structure with local polarization vector \mathbf{P} (b) oriented polymer chain with angle θ in the thin film coordinate system XY .

We simplify the stress gradient terms arising in Eq. (26) using Eq. (1a) and move the terms due to piezoelectricity and electrostriction to the right hand side. In this manner we seek the solution in the mechanical deformation with distributed electrical source. For example, the linear components on the right-hand electrical source term are written as

$$f_x = -e_{31} \frac{\partial E_z}{\partial x} - e_{36} \frac{\partial E_z}{\partial y}, \quad f_y = -e_{36} \frac{\partial E_z}{\partial x} - e_{32} \frac{\partial E_z}{\partial y}, \quad f_z = -e_{33} \frac{\partial E_z}{\partial y}. \quad (28a)$$

Note that here f_x , f_y and f_z are functions of the transverse electric field E_z only. This is due to the particular form of piezoelectric coupling and the electric field approximation for the thin film, i.e., $E_z = -\partial\Phi(x, y)/\partial z$ with $\Phi(x, y)$ as the applied voltage. This is a reasonably simple type of electromechanical coupling (apart from the nonlinear parts), yet an important one to analyze the in-plane deformation and shear bands

The electric field has to satisfy Maxwell equations which are expressed as

$$\nabla \times \mathbf{E} = -\dot{\mathbf{B}}, \quad (29a)$$

$$\nabla \times \mathbf{H} = \dot{\mathbf{D}} + \sigma_c \mathbf{E} + \mathbf{J}_{\text{total}}, \quad (29b)$$

$$\nabla \cdot \mathbf{D} = \rho_{\text{total}}, \quad (29c)$$

$$\nabla \cdot \mathbf{B} = 0, \quad (29d)$$

where \mathbf{B} is the magnetic induction given by $\mathbf{B} = \mu \mathbf{u} \mathbf{H}$. The associated general impedance boundary conditions are

$$\mathbf{n} \times (\mathbf{E} - \mathbf{E}_{\perp}) = -\mathbf{J}_{sm}, \quad \mathbf{n} \times (\mathbf{H} - \mathbf{H}_{\parallel}) = \mathbf{J}_s \quad (30a)$$

at surfaces $z_{\perp} = -h/2, +h/2$, and

$$\mathbf{n} \cdot \mathbf{D} = \rho_s, \quad \mathbf{n} \cdot \mathbf{B} = 0 \quad (30b)$$

at the surfaces. Here, ρ_s as the surface charge, \mathbf{n} is the unit outward surface-normal.

By using the constitutive model derived in Sec. 2, Maxwell's equations in (29a)-(29d) are combined into the following system of coupled hyperbolic equations

$$\mu\epsilon \frac{\partial^2 \mathbf{E}}{\partial t^2} + \sigma_c \mu \frac{\partial \mathbf{E}}{\partial t} - \nabla^2 \mathbf{E} + \epsilon^{-1} \nabla \rho_{\text{total}} + \mu \mathbf{j}_{\text{total}} + \epsilon^{-1} \nabla \nabla \cdot [\mathbf{P}(\epsilon, \mathbf{E})] - \mu \frac{\partial^2}{\partial t^2} [\mathbf{P}(\epsilon, \mathbf{E})], \quad (31a)$$

$$\mu\epsilon \frac{\partial^2 \mathbf{H}}{\partial t^2} + \sigma_c \mu \frac{\partial \mathbf{H}}{\partial t} - \nabla^2 \mathbf{H} = -\nabla \times \mathbf{J}_{\text{total}} + \nabla \times \frac{\partial}{\partial t} [\mathbf{P}(\epsilon, \mathbf{E})]. \quad (31b)$$

Eqs. (31a)-(31b) can further be expressed in concise form, as

$$\mu\epsilon \frac{\partial^2 \mathbf{E}}{\partial t^2} + \sigma_c \mu \frac{\partial \mathbf{E}}{\partial t} - \nabla^2 \mathbf{E} = \mathbf{g}^E, \quad (32a)$$

$$\mu\epsilon \frac{\partial^2 \mathbf{H}}{\partial t^2} + \sigma_c \mu \frac{\partial \mathbf{H}}{\partial t} - \nabla^2 \mathbf{H} = \mathbf{g}^H, \quad (32b)$$

where the components of the right-hand-side represents the source terms due to deformation, hysteresis and charge transport, and they are coupled with Eq. (26). When the hysteresis and charge transport is absent, one could write

$$g_x^E = \epsilon_{11}^{-1} \frac{\partial^2 \bar{P}}{\partial x \partial z}, \quad g_y^E = \epsilon_{22}^{-1} \frac{\partial^2 \bar{P}}{\partial y \partial z}, \quad g_z^E = \epsilon_{33}^{-1} \frac{\partial^2 \bar{P}}{\partial z^2} - \mu_{33} \frac{\partial^2 \bar{P}}{\partial t^2}, \quad (33a)$$

$$g_x^H = \frac{\partial^2 \bar{P}}{\partial y \partial t}, \quad g_y^H = -\frac{\partial^2 \bar{P}}{\partial x \partial t}, \quad g_z^H = 0, \quad (34a)$$

and \bar{P} is the effective polarization (a scalar quantity) due to piezoelectricity, which is given by

$$\bar{P} = e_{31}\varepsilon_{xx} + e_{32}\varepsilon_{yy} + e_{33}\varepsilon_{zz} + e_{36}\varepsilon_{xy}. \quad (35)$$

We solve the coupled system of hyperbolic equations (26), (32a) and (32b), supplemented by associated boundary conditions, in $\{\mathbf{u}, \mathbf{E}, \mathbf{H}\}$ by finite element discretization. Charge transport and kinetics of the flow have not been coupled with the present model. Due to the geometry $(x, y, z) \in [0, L_x] \times [0, L_y] \times [-h/2, h/2]$ and the thin film limit ($h \rightarrow 0$), we choose the following form of the electromagnetic field

$$\mathbf{E} = \begin{Bmatrix} E(x, y)_x \\ E(x, y)_y \\ -(z/h^2)\Phi(x, y) \end{Bmatrix}, \quad \mathbf{H} = \begin{Bmatrix} H(x, y)_x \\ H(x, y)_y \\ 0 \end{Bmatrix}, \quad (36a)$$

where $\Phi(x, y)$ is the potential between the parallel surface electrodes. Distribution of the potential can be prescribed for electrical excitation and the system can be solved for \mathbf{u}_{ep} and $\{E_x E_y H_x H_y\}$, whereas for mechanical actuation we solve the system for \mathbf{u}_{ep} and $\{E_x E_y \Phi H_x H_y\}$.

5. NUMERICAL SIMULATIONS

COMSOL multiphysics modelling software package¹¹ has been used for finite element simulation with right-hand side coupling terms in the governing partial differential differential equations. P(VDF-TrFE) copolymer blend with araldite is considered. PZT is considered as the piezoelectric particulate phase. A square film geometry of size $L_x = L_y = 0.05m$ and thickness $h = 2mm$ is discretized by tetrahedral Lagrangian finite element with second order accurate time stepping scheme. A deterministic distribution of chains angles θ has been used, which is given by

$$\theta(x_i, y_i)_i = \frac{\pi}{4} \left[\frac{x_i(L_x - x_i)}{L_x^2} + \frac{y_i(L_y - y_i)}{L_y^2} \right], \quad \theta(x_i, y_i)_i^0 = 0. \quad (37)$$

Material properties are used from the published literature (see^{4, 12}). Effects of increase in the copolymer volume fraction on the deformation under mechanical loading are analyzed below. We apply a sinusoidal displacement of amplitude $2.5mm$ uniformly and normal to the parallel edges $x = 0, L_x$. Time period of the applied displacement history is taken as $T_u = 10s$. For the first sample we consider $\nu_{co} = 0.2$, $a = 0.8$, $n = 8.5$ which represents a predominantly piezoelectric composite film. Figs. 3(a) and (b) show the contours of longitudinal displacement u_1 and lateral displacement u_2 , respectively, at $t = T_u/4$. Figs. 3(c) and (d) show the longitudinal strain ε_{xx} and the lateral strain ε_{yy} contours, respectively for the same composition. These figures reveal usual deformation patterns for the piezoelectric composite at the mesoscopic and macroscopic scales. Next we increase the copolymer volume fraction to $\nu_{co} = 0.5$ with $a = 0.5$, $n = 8.5$. Fig. 4(a) shows the u_1 contours at $t = T_u/8$ which indicates tensile load initiation. In this figure, a large pair of deformation gradients parallel to the loaded edges can be seen. Such deformation gradients were not observed for the composition with high piezoelectric particulate and low copolymer volume fraction. Figs. 4(b) and (c) show u_1 and u_2 contours at $t = T_u/4$ which also indicate fully developed strain gradient zones. Comparing these two figures with Figs. 3(a) and (b) for the low copolymer high piezoelectric particulate composition, we observe that an increase in the copolymer volume fraction leads to specific shape of the strained region with high amount of flow, which is due to the stretching of the copolymer chains. From the Figs. 4(d) and (e) of strain contours, we can clearly observe the diagonally oriented patterns of

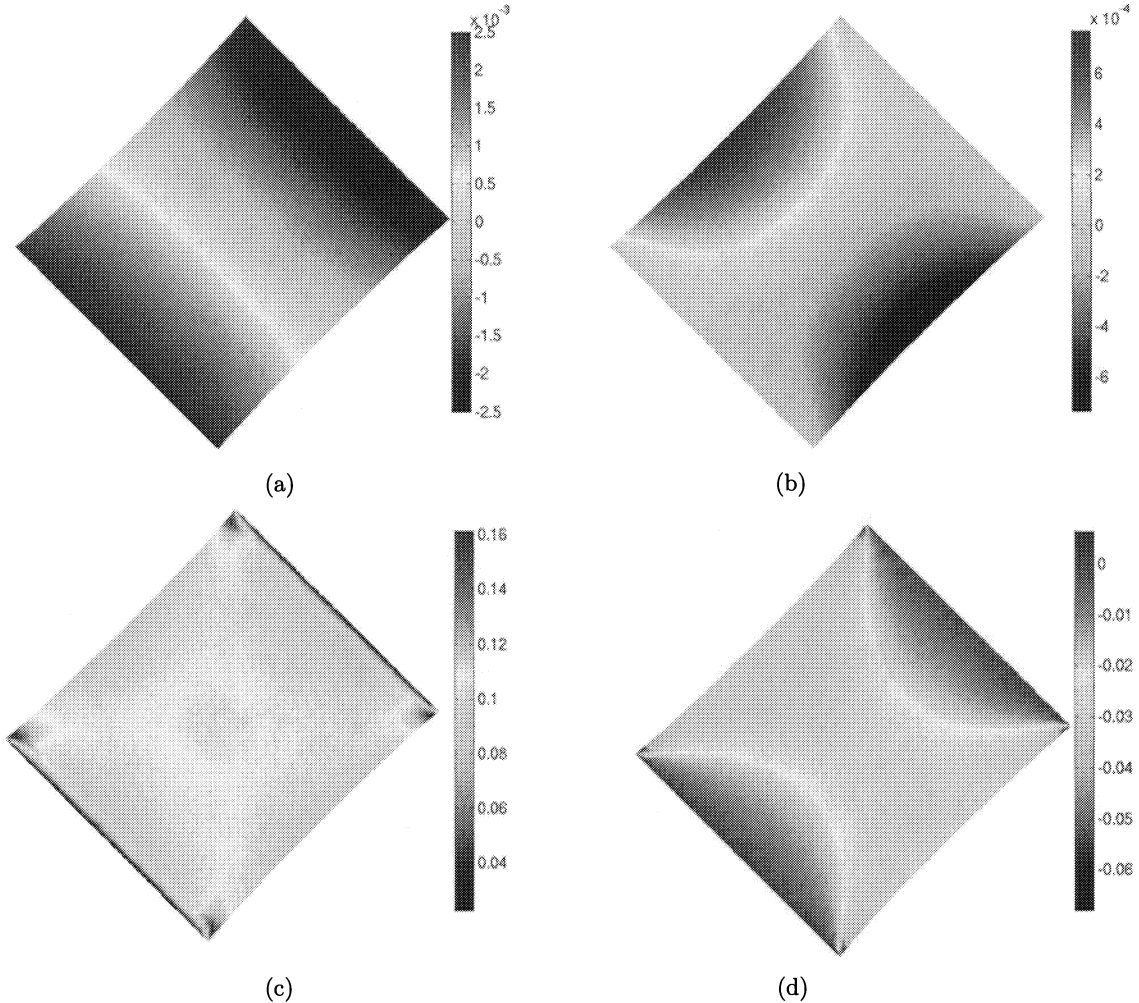


Figure 3. (a) Longitudinal displacement u_1 (b) lateral displacement u_2 (c) longitudinal strain ϵ_{xx} and (d) lateral strain ϵ_{yy} contours at $t = T_u/4$. Volume fraction of copolymer is 0.2, $a = 0.8$.

principle strains. With these strained patterns we also see one order higher magnitude compared to the continuous patterns of the principle strains observed in case of low piezoelectric and high piezoelectric composition (see Figs. 3(c) and (d)).

6. CONCLUSIONS

A mesoscopic model to analyze various effects of electroactive and flow related properties in piezoelectric copolymer composite thin film has been developed in this paper. The three-phase constitutive model takes into account the local transport of cations for ionic polymer, electrostriction and anhysteretic polarization within a simple constitutive averaging scheme. A finite strain description is given to model the kinematics of the copolymer chains. Finite element simulation is carried out by considering a P(VDF-TrFE)-PZT-Araldite thin film. Increasing copolymer content substantially changes the deformation pattern in the film.

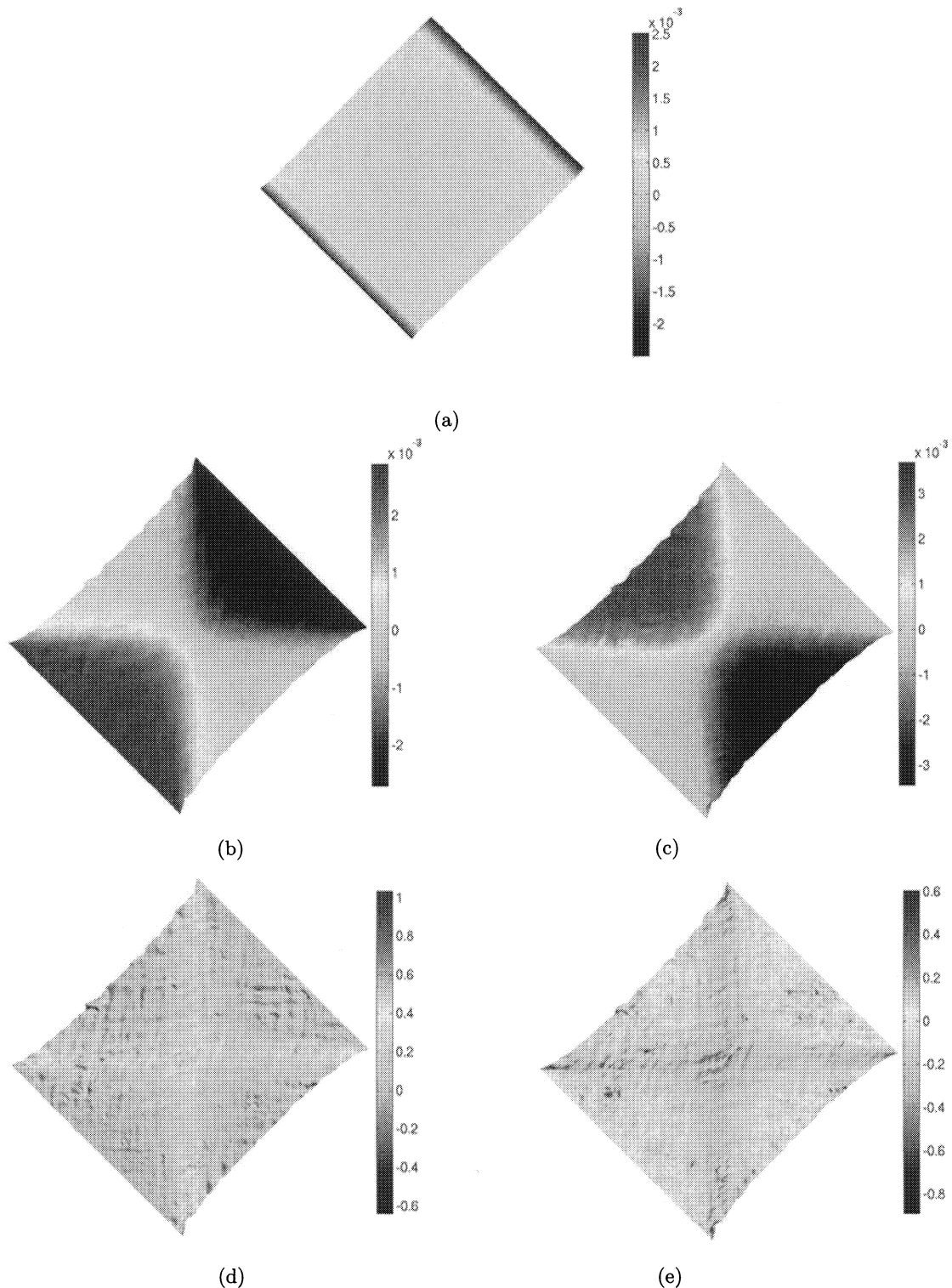


Figure 4. (a)Longitudinal displacement u_1 contour at $t = T_u/8$. Longitudinal displacement u_1 (b) lateral displacement u_2 (c) longitudinal strain ϵ_{xx} and (d) and lateral strain ϵ_{yy} contours at $t = T_u/4$. Volume fraction of copolymer is 0.5, $a = 0.5$.

REFERENCES

1. S. Palto, L. Blinov, A. Bune, E. Dubovik, V. Fridkin, N. Petukhova, K. Verkhovskaya, and S. Yudin, "Ferroelectric langmuir-blodgett films," *Ferroelectric Lett.* **19**, p. 65, 1995.
2. M. Shahinpoor, "Inonic polymer-conductor composite as biomimetic sensors, robotic actuators and artificial muscles - a review," *Electrochimica Acta* **48**, pp. 2343–2353, 2003.
3. R. Pehrine, R. Kornbluh, and J. Joseph, "Electrostriction of polymer dielectrics with compliant electrodes as a means of actuation," *Sensors and Actuators A: Phys.* **64**, pp. 77–85, 1999.
4. J. Harrison and Z. Ounaies, "Piezoelectric polymers," *ICASE Report No. 2001-43 NASA/CR-2001-211422*, pp. 1–26, 2001.
5. T. Furukawa, "Structure and functional properties of ferroelectric polymer," *Advan. Colloid and Interface Sci.* **1997**, pp. 183–308, 1997.
6. T. S. Chow, *Mesoscopic Physics of Complex Materials*, Springer-Verlag, NY, 2000.
7. J. D. Carbeck and G. C. Rutledge, "Temperature dependent elastic, piezoelectric and pyroelectric properties of β -poly(vinylidene fluoride) from molecular simulation," *Polymer* **37(22)**, pp. 5089–5097, 1996.
8. J. A. Young, B. L. Farmer, and J. A. Hinkley, "Molecular modeling of the poling of piezoelectric polyamides," *Polymer* **40**, pp. 2787–2795, 1999.
9. H. Banno and S. Saito, "Piezoelectric and dielectric properties of composites of synthetic rubber and PbTiO_3 or PZT ," *J. Appl. Phys.* **22(2)**, p. 67, 1983.
10. R. C. Smith and C. L. Hom, "A domain wall theory of ferroelectric hysteresis," *J. Intelligent Mater. Sys. Struct.* **10(3)**, pp. 195–213, 1999.
11. C. AB, *COMSOL Multiphysics User's Guide*, Burlington, MA, 2005.
12. T. E. Gomez, F. M. Espinosa, F. Levassort, M. Lethiecq, A. James, E. Ringgard, C. E. Millar, and P. Hawkins, "Ceramic powder-polymer piezocomposites for electroacoustic transduction: modeling and design," *Ultrasonics* **36**, pp. 907–923, 1998.

Contents

Volume 6168: Smart Structures and Materials 2006: Electroactive Polymer Actuators and Devices (EAPAD)

PLENARY SESSION

EAP AS EMERGING ACTUATORS AND BIOMIMETIC TECHNOLOGIES

ELECTRONIC EAP I

ELECTRONIC EAP II

NEW AND OTHER EAP INCLUDING PAPER, PROTEIN, ETC. I

NEW AND OTHER EAP INCLUDING PAPER, PROTEIN, ETC. II

IONIC EAP: CONDUCTIVE/CONJUGATED POLYMER AND NANOTUBES

IPMC AS EAP I

IPMC AS EAP II

APPLICATIONS OF EAP: ROBOTICS, MEDICAL, ETC.

MODELING IPMC AND OTHER IONIC EAP

TRANSDUCING EFFECTS IN EAP

TRANSDUCING EAP

APPLICATIONS OF EAP

POSTER SESSION

Volume 6169: Smart Structures and Materials 2006: Damping and Isolation

ACTIVE CONTROL

SHUNTED PIEZOS

ENERGY HARVESTING

MAGNETORHEOLOGICAL FLUIDS

PASSIVE DAMPING

VIBRATION ISOLATION

DAMPING WITH NANOTUBES AND NANOPARTICLES

ADAPTIVE AND TUNABLE DAMPING

POSTER SESSION

Volume 6170: Smart Structures and Materials 2006: Active Materials: Behavior and Mechanics

FERROELECTRICS I

FERROELECTRICS II

Contents

FERROELECTRICS III
MAGNETOSTRICTIVES I
MAGNETOSTRICTIVES II
SMA/FMSM I
SMA/FMSM II
SMA/FMSM III
MULTIFUNCTIONAL COMPOSITES II
MULTIFUNCTIONAL COMPOSITES III
MULTIFUNCTIONAL POLYMERS
POSTER SESSION

Volume 6171: Smart Structures and Materials 2006: Industrial and Commercial Applications of Smart Structures Technologies

POWER GENERATION AND TRANSMISSION
PIEZOELECTRIC DEVICES (DRILLS, PUMPS, ETC.)
QUALITY AND PROCESS CONTROL
MAGNETO RHEOLOGICAL FLUIDS
SMART STRUCTURES AND MATERIALS, AND NOISE REDUCTION

Volume 6172: Smart Structures and Materials 2006: Smart Electronics, MEMS, BioMEMS, and Nanotechnology

SIMULATION AND MODELING
NOVEL MATERIALS AND INTEGRATION TECHNIQUES I
NOVEL MATERIALS AND INTEGRATION TECHNIQUES II
NANOSTRUCTURES
RF MEMS AND WIRELESS COMMUNICATION DEVICES
INTEGRATED NANO- AND MICRO-STRUCTURES I
INTEGRATED NANO- AND MICRO-STRUCTURES II
PACKAGING
INTEGRATED NANO- AND MICRO-STRUCTURES III
PACKAGING AND APPLICATIONS OF MEMS TO SMART SYSTEMS
APPLICATIONS

Effect of reduction temperature on electrode formation and performance of ionic polymer metal composites [6168-75]

J. Lee, K. Vinh, S. Park, Y. Yoo

Viscoelastic study of conducting polymers using quartz crystal microbalance [6168-77]

M. Bahrami Samani, P. Whitten, G. Spinks, C. Cook

Multiple electrode patterning of ionic polymer metal composite actuators [6168-78]

I. Oh, J. Jeon, Y. Lee

Application of the Monte Carlo method for creation of initial models of EAP molecules for molecular dynamics simulation [6168-80]

E. Soolo, J. Karo, H. Kasemägi, M. Kruusmaa, A. Aabloo

Digital pulse-activated cell pump [6168-82]

M. Banister, S. Vohnout

Mesoscopic dynamics of piezoelectric copolymer thin films [6168-83]

D. Mahapatra, R. Melnik

Synthesis of new solid polymer electrolyte and actuator based on PEDOT/NBR/ionic liquid [6168-84]

M. Cho, H. Seo, J. Nam, H. Choi, J. Koo, Y. Lee

Effect of bending stiffness of the electroactive polymer element on the performance of a hybrid actuator system (HYBAS) [6168-87]

T. Xu, J. Su, X. Jiang, P. Rehrig, S. Zhang, T. Shrout, Q. Zhang

Polyppyrrole actuators for micropump applications [6168-88]

J. Travas-Sejdic, R. Kiefer, S. Valiavalappil, K. Li, P. Kilmartin

New design concept for dielectric elastomer actuators [6168-89]

G. Kofod, M. Paajanen, S. Bauer

Electromechanical characterization and measurement protocol for dielectric elastomer actuators [6168-90]

S. Bauer, M. Paajanen

Volume 6169: Smart Structures and Materials 2006: Damping and Isolation

Chairs/Editors: William W. Clark, Mehdi Ahmadian, Arnold Lumsdaine

Conference Committee

Symposium Committee

ACTIVE CONTROL

PVDF control of piezoelectric tube scanners [6169-1]

B. Bhikkaji, M. Ratnam, S. Moheimani

Electromagnetic films as lightweight actuators for active noise reduction [6169-3]

D. Sachau, T. Kletschkowski

H-infinity controller design for structural damping [6169-4]

D. Rowen, M. Hopkins

SHUNTED PIEZOS

Improved self-sensing method for semi-active vibration suppression [6169-7]

K. Makihara, J. Onoda, K. Minesugi

PROCEEDINGS OF SPIE on CD-ROM

Smart Structures and Materials 2006

26 February–2 March 2006
San Diego, California USA



The International Society
for Optical Engineering

Volumes 6166–6174

Single-User Edition

